blood advances

American Society of Hematology
2021 L Street NW, Suite 900,
Washington, DC 20036
Phone: 202-776-0544 | Fax 202-776-0545
bloodadvances@hematology.org

Proteogenomic features define subtypes of mantle cell lymphoma

Tracking no: ADV-2025-018701R1

Yuting Yan (State Key Laboratory of Experimental Hematology, Institute of Hematology & Blood Diseases Hospital, Chinese Academy of Medical Science & Peking Union Medical College, China) Weihao Chen (State Key Laboratory of Experimental Hematology, Institute of Hematology & Blood Diseases Hospital, Chinese Academy of Medical Science & Peking Union Medical College, China) Xinzhou Ge (Department of Statistics, University of California, United States) Jian Sun (Peking Union Medical College Hospital,) Lei Yu (Department of Botany and Plant Sciences, University of California, United States) Krystine Garcia-Mansfield (Translational Genomics Research Institute, United States) Xinyi Zhang (State Key Laboratory of Experimental Hematology, National Clinical Research Center for Blood Diseases, Haihe Laboratory of Cell Ecosystem, Institute of Hematology & Blood Diseases Hospital, Chinese Academy of Medical Sciences & Peking Union Medical College, China) Ying Yu (State Key Laboratory of Experimental Hematology, National Clinical Research Center for Blood Diseases, Institute of Hematology & Blood Diseases Hospital, Chinese Academy of Medical Sciences & Peking, China) Wenjie Xiong (State Key Laboratory of Experimental Hematology, Institute of Hematology & Blood Diseases Hospital, Chinese Academy of Medical Science & Peking Union Medical College, China) Dehui Zou (State Key Laboratory of Experimental Hematology, National Clinical Research Center for Blood Diseases, Haihe Laboratory of Cell Ecosystem, Institute of Hematology & Blood Diseases Hospital, Chinese Academy of Medical Sciences & Peking Union Medical College, Tianjin, China, China) Gang An (State Key Laboratory of Experimental Hematology, National Clinical Research Center for Blood Diseases, Haihe Laboratory of Cell Ecosystem, Institute of Hematology & Blood Diseases Hospital, Chinese Academy of Medical Sciences & Peking Union Medical College, China) Zhenyu Jia (Department of Botany and Plant Sciences, University of California, United States) Patrick Pirrotte (The Translational Genomics Research Institute, United States) Jessica Li (Department of Statistics, University of California, United States) Zhen Yu (State Key Laboratory of Experimental Hematology, Institute of Hematology & Blood Diseases Hospital, Chinese Academy of Medical Science & Peking Union Medical College, China) Mu Hao (Blood hospital and hematology institute, state key lab of experimental hematology, China) Lugui Qiu (State Key Laboratory of Experimental Hematology, National Clinical Research Center for Hematological Disorders, Institute of Hematology and Blood Diseases Hospital, Chinese Academy of Medical Sciences, China) Jianwei Qi (State Key Laboratory of Experimental Hematology, National Clinical Research Center for Blood Diseases, Haihe Laboratory of Cell Ecosystem, Institute of Hematology & Blood Diseases Hospital, Chinese Academy of Medical Sciences & Peking Union Medical College, China) Lili Wang (Columbia University Irving Medical Center, United States) Shuhua Yi (Institute of Hematology and Blood Disease Hospital, Chinese Academy of Medical Sciences and Peking, China)

Abstract:
Mantle cell lymphoma (MCL) is a biologically heterogeneous B-cell malignancy. While genomics and transcriptomics have delineated parts of the MCL disease spectrum, the proteomics remains largely unexplored. Here, we conducted a comprehensive proteogenomic analysis integrating genomics, transcriptomics, and proteomics on peripheral blood samples from 27 MCL patients and 4 healthy donors to investigate the translational and post-translational dimensions of MCL. Our study identified 1,296 downregulated and 468 upregulated proteins in MCL cells. The splicing pathways were significantly upregulated at both the mRNA and protein levels, suggesting a critical role for aberrant RNA splicing in MCL pathogenesis. Integration of proteomic data with genetic aberrations revealed IGHV mutational status and CCND1 mutation are associated with distinctive transcriptomic and proteomic profiles, which correspond to significant differences in clinical outcomes. A multi-omics molecular stratification model incorporating proteomic data showed superior predictive power for patient survival compared to single-omics models (concordance index 0.83 vs. 0.74). This study provides the first comprehensive proteogenomic profile of MCL, offering novel insights into its molecular mechanisms and clinical behavior. The identification of molecular subtypes and prognostic protein signatures underscores the potential of proteomics to guide precision medicine strategies for MCL.

Conflict of interest: No COI declared

COI notes:

Preprint server: No;

Author contributions and disclosures: SHY and LLW conceptualized the study design. YTY collected samples, performed experiment and created graphs, WHC and YTY wrote the manuscript. YYT, XZG, JS, JL, MK, and PP conducted data analysis and statistics. XYZ, YY, TYW, WJX, DHZ, GA, MH, and ZY acquired the data and managed the patients. LLW, LGQ, JWQ and SHY revised the manuscript critically and approved the final version.

Non-author contributions and disclosures: No;

Agreement to Share Publication-Related Data and Data Sharing Statement: The WES and RNA-seq data for the 27 MCL patients were previously published in GSA database (BioProject ID PRJCA028747). The mass spectrometry proteomics data generated in this study have been deposited in the ProteomeXchange Consortium via the iProX partner repository with the dataset identifier PXD066628 (URL for reviewers: https://www.iprox.cn/page/SSV024.html;url=1758509803879RPri, Password: bk8J).

Clinical trial registration information (if any):

Proteogenomic features define subtypes of mantle cell lymphoma

Yuting Yan[1,2]*, Weihao Chen[1,2]*, Xinzhou Ge[3,4]*, Jian Sun[5]*, Lei Yu[6,7], Krystine Garcia-Mansfield[8,9], Xinyi Zhang[1,2], Ying Yu[1,2], Wenjie Xiong[1,2], Dehui Zou[1,2], Gang An[1,2], Zhenyu Jia[6], Patrick Pirrotte[8,9], Jessica Jingyi Li[3,4], Zhen Yu[1,2], Mu Hao[1,2], Lugui Qiu[1,2#], Jianwei Qi[1,2#], Lili Wang[10,11#], Shuhua Yi[1,2#] for the Chinese Workshop of Indolent Lymphomas

[1.] State Key Laboratory of Experimental Hematology, National Clinical Research Center for Blood Diseases, Haihe Laboratory of Cell Ecosystem, Institute of Hematology & Blood Diseases Hospital, Chinese Academy of Medical Sciences & Peking Union Medical College, Tianjin 300020, China.

[2.] Tianjin Institutes of Health Science，Tianjin 301600, China.

[3.] Department of Statistics, University of California, Los Angeles, California.

[4.] Department of Computational Medicine, University of California, Los Angeles, California.

[5.] Peking Union Medical College Hospital, Chinese Academy of Medical Sciences and Peking Union Medical College, Beijing, China.

[6.] Department of Botany and Plant Sciences, University of California, Riverside, California.

[7.] Graduate Program in Genetics, Genomics, and Bioinformatics, University of California, Riverside, California.

[8.] Cancer & Cell Biology Division, Translational Genomics Research Institute, Phoenix, Arizona, USA.

[9.] Integrated Mass Spectrometry Shared Resource, City of Hope Comprehensive Cancer Center, Duarte, California, USA.

[10.] Department of Systems Biology, Beckman Research Institute, City of Hope National Comprehensive Cancer Center, Monrovia, California.

[11]. Division of Hematology & Oncology, Columbia University Medical Center, New York, New York.

*[#] Equal contributors

Correspondence:

Shuhua Yi,

288 Nanjing Road, Tianjin 30020, China. yishuhua@ihcams.ac.cn

Lili Wang,

630 W 168th St, NY 10032. lw3282@cumc.columbia.edu

Jianwei Qi,

288 Nanjing Road, Tianjin 30020, China. qijianwei@ihcams.ac.cn

Lugui Qiu,

288 Nanjing Road, Tianjin 30020, China. qiulg@ihcams.ac.cn

Running title: Proteogenomic Landscape of Mantle Cell Lymphoma

Data availability: The WES and RNA-seq data for the 27 MCL patients were previously published in GSA database (BioProject ID PRJCA028747).

The mass spectrometry proteomics data generated in this study have been deposited in the ProteomeXchange Consortium via the iProX partner repository with the dataset identifier PXD066628 (URL for reviewers: https://www.iprox.cn/page/SSV024.html;url=1758509803879RPri, Password: bk8J).

Abstract

Mantle cell lymphoma (MCL) is a biologically heterogeneous B-cell malignancy. While genomics and transcriptomics have delineated parts of the MCL disease spectrum, the proteomics remains largely unexplored. Here, we conducted a comprehensive proteogenomic analysis integrating genomics, transcriptomics, and proteomics on peripheral blood samples from 27 MCL patients and 4 healthy donors to investigate the translational and post-translational dimensions of MCL. Our study identified 1,296 downregulated and 468 upregulated proteins in MCL cells. The splicing pathways were significantly upregulated at both the mRNA and protein levels, suggesting a critical role for aberrant RNA splicing in MCL pathogenesis. Integration of proteomic data with genetic aberrations revealed IGHV mutational status and *CCND1* mutation are associated with distinctive transcriptomic and proteomic profiles, which correspond to significant differences in clinical outcomes. A multi-omics molecular stratification model incorporating proteomic data showed superior predictive power for patient survival compared to single-omics models (concordance index 0.83 vs. 0.74). This study provides the first comprehensive proteogenomic profile of MCL, offering novel insights into its molecular mechanisms and clinical behavior. The identification of molecular subtypes and prognostic protein signatures underscores the potential of proteomics to guide precision medicine strategies for MCL.

Key Points:

We present the first comprehensive proteogenomic analysis of MCL, integrating proteomics with matched WES and RNA-seq data.

We identified four molecular subtypes with distinct features, which demonstrate superior prognostic value compared with genomics alone.

Introduction

The molecular landscape of Mantle cell lymphoma (MCL) has been extensively characterized by whole-exome sequencing (WES) and transcriptome analysis, uncovering numerous recurrent genetic alterations and gene expression changes that contribute to biological heterogeneity of MCL (1-6). However, genomic and transcriptomic data alone do not fully capture the complex proteomic landscape that ultimately determines cellular behavior. Proteins, as the functional effectors of cellular processes, have traditionally been studied indirectly through mRNA measurements. Recent advances in mass spectrometry (MS)-based proteomics have allowed direct investigation of the post-transcriptional landscape across various tumors (7-12). Such approaches have enabled the discovery of distinct molecular subtypes, the elucidation of oncogenic mechanisms, and the identification of therapeutic vulnerabilities. In MCL, most protein-level studies to date have been limited to targeted immunoblotting of selected proteins, lacking a global view of the proteome. A comprehensive and unbiased survey of proteomics in MCL is thus urgently needed.

To address this knowledge gap, we conducted a proteogenomic analysis in primary MCL samples and explored the relationships among genetics, transcriptomics, and proteomics of MCL. Building on our previous study, in which we characterized the genomic landscape of 134 MCL patients and identified four robust genetic subtypes (5), the current study focuses on a representative subset of 27 patients from that cohort for whom sufficient biospecimens were available for deep proteomic profiling.

Methods

Human samples

Normal samples were obtained from peripheral blood (PB) of 4 healthy donors, while tumor samples were collected from PB of 27 newly diagnosed MCL patients with PB involvement. All patients and healthy donors were male. All MCL cases harbored the characteristic t(11;14)(q13;q32) translocation with cyclin D1 overexpression and were diagnosed according to WHO criteria. The entire protocols were approved by the Human Subjects Protection Committee of the Institute of Hematology and Blood Disease Hospital, the Chinese Academy of Medical Sciences, and the Peking Union Medical College Ethics Committees. All studies were performed after obtaining written informed consent from the patients and in accordance with the Declaration of Helsinki. Mononuclear cells from PB were

isolated by density gradient centrifugation using Ficoll-Paque Medium (GE Healthcare). Normal B cells and MCL tumor cells were enriched using CD19 magnetic beads followed by flow cytometry-based sorting prior to protein extraction.

Proteomic analysis

Proteomic profiling was performed using data-independent acquisition mass spectrometry (DIA-MS). Proteins were extracted, reduced, alkylated, acetone-precipitated, and digested with trypsin following standard protocols. Peptides were desalted, lyophilized, and analyzed on an EASY-nLC™ 1200 UHPLC system (Thermo Fisher Scientific) coupled to an Orbitrap Q Exactive mass spectrometer (Thermo Fisher Scientific), operating in DIA mode. Protein identification and quantification were performed using Proteome Discoverer 2.2 (Thermo Fisher Scientific) and Spectronaut™ 9.0 (Biognosys) with a false discovery rate (FDR) of 1%. Label-free quantification was conducted using the MaxLFQ algorithm. More protein extraction processes were present in supplementary methods.

Integrative data analysis

Proteomic data preprocessing and missing value imputation were performed using the R package “DEP”. Weighted gene co-expression network analysis (“WGCNA” package) was applied to both proteomic and transcriptomic data, with the soft-thresholding power selected based on mean connectivity. Gene Ontology and gene set enrichment analysis (GSEA) were conducted using the R package “clusterProfiler”, with a q-value < 0.05 considered significant.

Differential expression analyses for RNA sequencing (RNA-seq) and proteomic data were performed using two-sample t-tests following Trimmed Mean of M-values and counts-per-million normalization, respectively. *P*-values were adjusted using the Benjamini–Hochberg method. To identify proteins associated with specific genetic variants, patients were first grouped according to the presence or absence of the variant, followed by differential protein expression analysis between the two groups under a target FDR of 5%.

We performed Similarity Network Fusion (SNF) method to integrate data from different omics layers for clustering and visualization (13), using the “ExecuteSNF.CC” package. The detailed clustering method is described in the supplementary materials.

Statistical considerations

Survival curves were plotted using the Kaplan-Meier method, and the log-rank test was applied to evaluate the statistical significance of progression-free survival (PFS) and overall survival (OS)

between different clusters. Multivariate Cox regression analysis was used to evaluate the independent prognostic value of the MCL International Prognostic Index (MIPI) risk system and individual protein signatures for clinical outcomes of MCL.

Ethics statement

All patients signed written informed consent for this study. The entire study procedure was conducted according to the Declaration of Helsinki and was approved by the Human Subjects Protection Committee of the Institute of Hematology and Blood Disease Hospital, the Chinese Academy of Medical Sciences, and the Peking Union Medical College Ethics Committees (KT2020025-EC-2).

Results

To explore the relationship between genotype and phenotype in MCL, we performed protein abundance measurements using MS in DIA mode and integrated these data with matching WES and RNA-seq data from matched samples (Figure 1A). The genomic and transcriptomic data for these 27 patients were obtained from our previously published study (5). The MCL cohort included 27 patients with a broad range of clinical characteristics (Table 1). All patients had bone marrow involvement at diagnosis. The median age was 57 years (range, 44–79 years), and the 3-year OS in this cohort was 37.5% (95% CI, 22.5%-62.5%), consistent with the inclusion of several high-risk cases.

Integrated proteogenomic and transcriptomic analysis identified key pathways associated with MCL biology

Across all samples, 5702 proteins were consistently detected. Differential analysis between MCL and normal B cells revealed extensive alterations (Figure 1B), with 468 proteins significantly upregulated and 1,296 downregulated in MCL (FDR<0.05). The hallmark oncoprotein CCND1 was among the most upregulated proteins. In addition, several novel or unexpected proteins related to cell metabolism and oxidative stress were overexpressed in MCL, such as NLRP3, HSDL1, and MRPL21. Conversely, adhesion and cytoskeletal regulators such as PARVB and FERMT3 were markedly downregulated. Functional enrichment analysis of the differentially expressed proteins showed distinct biological themes (Figure 1C). Upregulated proteins were enriched in DNA replication/repair, cell cycle, RNA splicing and processing, and metabolism. This indicates that MCL cells have an enhanced capacity for genome maintenance, transcription/translation processes, and metabolic

activity. Contrarily, downregulated proteins were involved in cellular structure, adhesion, immune response, cell–cell interaction, and MAPK signaling. The loss or reduction of these pathways suggests that MCL cells may have defects in immune surveillance and cell adhesion, potentially facilitating immune evasion and dissemination in the body.

We integrated matched RNA-seq and proteomic data to assess how closely mRNA changes mirror protein changes. For each biological pathway, we compared the enrichment trends at the mRNA and protein levels. A comparison of pathway activity changes between transcriptome and proteome shows a mixed pattern (Pearson correlation r=0.449, P<0.01, Figure S1). While some pathways are concordantly upregulated or downregulated at both mRNA and protein levels, many pathways exhibit discordant changes. For instance, the SWI/SNF chromatin-remodeling complex was significantly upregulated at the protein but not mRNA level, whereas pathways such as gap junction assembly were enriched at the transcript level but not at the protein level, suggesting post-transcriptional regulation in these pathways (Figure S1). We identified 65 consistently upregulated and 148 consistently downregulated genes at both mRNA and protein levels in MCL (Figure 1D). Co-upregulated genes were primarily enriched in splicing and DNA replication pathways, while co-downregulated genes were linked to actin cytoskeleton regulation and chemokine signaling (Figure 1E). Notably, the spliceosome pathway showed strong and consistent upregulation at both RNA and protein levels (Figure 1F and S2). Detailed examination of the spliceosome components revealed that most core spliceosomal proteins and associated splicing factors (e.g., SF3A2, SF3B4, SNRPB, U2AF1, and DDX39B) were uniformly elevated in MCL cells (Figure S3), indicating that aberrant RNA splicing is a pervasive feature of MCL biology.

Proteogenomic associations with genetic lesions in MCL

We investigated the impact of recurrent genetic aberrations on the MCL proteome. Seventeen lesions were considered: 10 regions of copy number variation (CNV) and 7 frequently mutated genes, based on prior genomic studies (2, 3, 5, 6). Comparing protein expression between samples with and without each genetic lesion revealed distinct proteomic signatures for key lesions (Figure 2A–B).

IGHV-mutated status exerted the strongest influence on the proteome, with numerous proteins differentially expressed between IGHV-mutated and IGHV-unmutated MCL. Compared to unmutated samples, IGHV-mutated samples showed upregulation of DNA damage response (ATM) and mitochondrial proteins (GLS2, PCK2, PPM1K) (Figure 2C). By contrast, IGHV-unmutated cases displayed upregulation of proteins implicated in cell cycle and DNA repair (CDK2, HMGB3), structural microtubule-associated proteins and chaperones (STMN1, SERPINH1, HSPA1B) (Figure 2C).

Further pathway enrichment analysis showed that IGHV-mutated tumors were enriched in metabolism (oxidative phosphorylation [OXPHOS], tricarboxylic acid cycle, alanine aspartate and glutamate metabolism, and adipogenesis). They also showed enrichment in B-cell receptor (BCR) signaling and antigen processing/presentation pathways, indicating that IGHV-mutated cells maintain B-cell functional programs and interactions with the immune system. Additionally, ribosomal proteins were enriched, suggesting robust protein synthesis in IGHV-mutated MCL. For IGHV-unmutated cells, significant enrichments were observed in proteasome, cell cycle, DNA damage regulation, spliceosome, glutathione metabolism, and interferon response (Figure 2D). These enrichments suggest that IGHV-unmutated cells exhibit a proliferative and stress-adapted phenotype.

CCND1 mutation also affected the proteome. Although *CCND1* translocation in essentially all classic MCL, somatic coding mutations of *CCND1* occur in a subset of cases and have been linked to a more indolent course in some studies (5). Mutations in *CCND1* were associated with FcγR-mediated phagocytosis and BCR signaling pathways (Figure 2E). This suggest that subsets of MCL defined by IGHV or *CCND1* status have unique proteomic and signaling profiles that could influence their behavior and therapy response.

To further investigate whether recurrent CNVs exert cis-regulatory effects on protein expression, a total of 297 CNV-protein pairs were analyzed, comprising proteins encoded by genes located within the respective CNV regions. We observed significant associations (P<0.05) for 126 pairs (42.4%), with 117 pairs (39.4%) remaining significant after FDR correction (FDR<0.1). 247 pairs (83.2%) exhibited the expected direction. This concordance rate was highly significant by binomial test (Figure S4, P<0.001). However, some genetic events occurred at a very low frequency, each observed in only three patients. Therefore, associations involving these alterations should be interpreted with caution and will require validation in larger cohorts.

mRNA-Protein concordance in MCL and its biological implications

To explore the relationship between mRNA abundance and protein abundance, we selected overlapping genes from two datasets, yielding 5222 mRNA-protein pairs, and calculated the Pearson correlation coefficient across the 27 MCL samples (Figure 3A). Overall, mRNA and protein levels showed a moderate correlation (r=0.377), indicating that although transcriptional control is operative, post-transcriptional regulation is also widespread.

By ranking genes according to mRNA-protein correlation coefficients (Figure 3B), we identified sets of genes at the extremes that offer insight into MCL biology. Genes with the highest positive correlations, including *DPYSL2*, *DBN1*, *RIN3*, *FAM120B*, *FLNB*, and *EPB41L2*, were mainly involved in

cytoskeletal organization, cell migration, membrane trafficking, and signaling. The tight mRNA-protein coupling suggests that in MCL cells, these cytoskeletal/migratory proteins are regulated mostly at the transcriptional level. In contrast, genes with the strongest negative correlations, including *MIS18BP1*, *SDHAF2*, *TDRD7*, *JMJD6*, *PCBP3*, and *BLM*, were related to DNA replication, chromatin regulation, and post-transcriptional regulation. The discordance of mRNA-protein suggests the robust post-transcriptional control. For example, their mRNAs may be present but translation is inhibited or proteins are rapidly degraded. We categorized genes according to their mRNA-protein correlation, defining high concordance as $r>0.6$ (n=825) and low concordance as $r<0.3$ (n=927). In total, genes with high mRNA-protein correlations were enriched in pathways related to mitotic spindle, immune response regulation, and signal transduction (Figure 3C). These are processes in which a concerted gene expression program may require the simultaneous production of many proteins, making transcriptional co-regulation effective. In contrast, most genes with low concordance were enriched in hallmark oncogenic pathways, such as MYC targets, DNA repair, and cell cycle (Figure 3D). This indicates that critical regulators of proliferation and genome integrity are subject to complex regulation beyond transcription in MCL. For instance, MYC-driven genes may be modulated by microRNAs or ubiquitin-mediated degradation, and many cell cycle or DNA repair proteins could be controlled by activation/inactivation rather than abundance.

Additionally, we observed that the degree of mRNA-protein correlation varied with MCL subtypes. Samples with blastoid/pleomorphic morphology had significantly higher overall mRNA-protein correlations than classic MCL, and IGHV-unmutated cases exhibited higher concordance than IGHV-mutated cases (Figure S5). These findings imply that more aggressive MCL operates with a more streamlined and efficient expression program, potentially meeting the demands of rapid proliferation. In comparison, indolent MCLs may tolerate more discordance, possibly reflecting the greater influence of regulatory checkpoints.

Prognostic signatures at the transcript and protein level

We next sought to identify genes and proteins with prognostic significance in our cohort and determine how the integration of multi-omics data could refine risk stratification in MCL. Despite the limited sample size, multiple candidate prognostic biomarkers were identified. At the mRNA level, we found 2980 RNAs associated with prognosis. Among them, APC2 and CCPG1, which are related to cell cycle and proliferation, were significantly associated with poor outcomes. FZD2 and RHOQP1, which are related to cell proliferation, differentiation, and motility, were significantly associated with better survival (Figure 4A). We note that these correlations do not imply causation, but can point to important biological differences. At the protein level, we identified 791 proteins associated with

prognosis, of which 493 were linked to inferior survival and 298 to favorable survival. Specifically, CNOT1/2, PCBP2, and CTR9, which are associated with post-transcriptional regulation and oncogene expression, showed significant correlations with inferior survival, whereas higher protein levels of RRAGC, TSG101, and RPS20, which are associated with tumor development, showed significant correlations with favorable survival (Figure 4B).

Intersecting transcript- and protein-level prognostic markers identified 252 genes with concordant prognostic significance at both levels (Figure 4C). This convergence provides higher confidence that these genes play a role in MCL progression. Among these genes, 141 were poor prognostic factors (hazard ratio [HR]>1; gene set A), and 92 were favorable prognostic factors (HR<1; gene set B) (Figure 4D). Pathway enrichment analysis revealed that gene set A was enriched in cell proliferation and DNA replication pathways (Figure 4E). Gene set B was enriched in ribosome, protein synthesis, and focal adhesion pathways, reflecting a more differentiated or stable cellular state that curbs aggressive (Figure 4E).

Integrative multi-omics clustering reveals four molecular subgroups

To explore the molecular heterogeneity of MCL, we first performed consensus clustering separately on proteomic and transcriptomic data. Using the partitioning around medoids algorithm with 500 bootstrap iterations, both omics layers stratified patients into three subgroups (Figure S6). However, suboptimal silhouette coefficients and limited concordance in cross-comparisons between the two single-omics classifications indicated insufficient stratification robustness (Table S1). These results suggest that single-omics approaches have limited power to robustly stratify MCL patients. Therefore, to integrate the multilayered molecular data and classify MCL patients into molecularly distinct subgroups, we subsequently developed a multi-omics integration model.

Through multivariate Cox regression analysis, we included key genetic lesions of 7 recurrent mutations and 10 CNVs, along with the top 300 survival-associated transcripts and the top 300 survival-associated proteins as input features for SNF clustering. Detailed survival statistics for the transcriptomic and proteomic features included in the model were listed in Table S2. We identified four clusters, designated C1 to C4, each defined by key driver genetic alterations, RNAs and proteins (Figure 5A). The average silhouette width for clustering was 0.78, indicating a robust separation among clusters (Figure S7A–B). Specifically, C1 was characterized by IGHV-mutated status, *CCND1* mutation, and absence of *del9p* or *del11q*; C2 correlated with *NSD2* mutation and higher MIPI scores; and C3 and C4 were more associated with *TP53* abnormalities and *del9p*, with *del1p21* particularly frequent in C3 (Figure 5A and Figure S7C). These findings were similar to those of our previous

WES-based study, where four genomic subgroups were also identified (5). In this study, patients in C1 group remained unchanged between single WES level and multi-omics level, reinforcing the robustness of this indolent subgroup. However, cases grouped C2–C4 by genomics alone were further distinguished into separate clusters upon multi-omics integration (Figure 5B). Four multi-omics clusters exhibited significantly different prognosis (OS, C1 to C4: not reached, 35.1, 19.0 and 12.5 months, P<0.001; PFS, C1 to C4: not reached, 22.7, 14.2 and 5.4 months, P<0.001; Figure 5C). The multi-omics model for assessing prognosis achieved a concordance index (C-index) of 0.83 for OS, which was higher than the C-index of 0.74 in the single-omics model. Using the cluster assignment as an ordinal risk score, the multi-omics clustering demonstrated superior discriminative ability for both OS (area under the curve [AUC]: 0.846 vs. 0.796) and PFS (AUC: 0.843 vs. 0.764) compared to single-omics clustering (Figure S8). Within this cohort, the multi-omics classification provided somewhat improved prognostic discrimination compared with the single-omics clustering. These findings are exploratory and require validation in larger independent series. Moreover, the protein signature remained independently prognostic after adjustment for MIPI risk. This suggests that these molecular subtypes capture risk that is not fully explained by clinical indices, highlighting a potential role for proteomic biomarkers in risk stratification.

To gain biological insight into each subgroup, cluster-specific GSEA was performed (Figure S9–S10). C1 demonstrated extensive enrichment of BCR-signaling pathways, consistent with antigen-experienced, ongoing BCR activity in these IGHV-mutated tumors. It also had high enrichment of OXPHOS, mitochondrial metabolism, ribosome, and mRNA translation pathways, indicating a metabolically active yet controlled proliferation. Immune-regulatory pathways were more active in C1, suggesting these tumors might have better interaction with immune cells. In C2, we observed moderate downregulation of cellular metabolic pathways unlike C1. However, RNA splicing, DNA replication, and immune-related pathways were slightly upregulated compared to C1. This cluster seems to occupy an intermediate biological state, not as metabolically active as C1, but without the severe suppression of BCR signaling and immune pathways seen in C3/C4. C3 was characterized by marked downregulation of BCR signaling, immune response, and apoptosis pathways. Meanwhile, C3 showed upregulation of OXPHOS, cell adhesion, and extracellular matrix interactions, which might indicate a tendency for these cells to reside in protective niches. C4 exhibited the most extreme profile, with significant downregulation of ribosome, BCR signaling, and immune-mediated pathways, coupled with notable upregulation of DNA replication/repair, P53, and cell cycle pathways.

We calculated RNA-protein correlation coefficients for each subgroup. We observed significantly discrepant correlation between RNA and protein expression across the subgroups. Interestingly, we noted a trend of increasing mRNA-protein correlation from C1 to C4 (Figure S11). This finding is consistent with our earlier observation (Figure S5) that aggressive MCL exhibits tighter transcriptional-translational coupling. In aggressive tumors, measuring either mRNA or protein might similarly capture the activity of critical pathways, whereas in indolent tumors, protein levels might provide additional information beyond mRNA due to greater post-transcriptional regulation.

Given the complexity and inapplicability of entire multi-omics grouping in practice, we developed a simplified multi-omics model. We performed differential expression analysis using the limma package to identify the top five differential factors in each cluster. From these results, we selected six DNA alterations, seven RNA transcripts, and three protein signatures that were biologically or clinically relevant to disease progression and tumor development. These features were then used to construct a simplified molecular classification model (Figure 5D). This parsimonious model successfully recapitulated the risk stratification of the full multi-omics analysis, achieving 100% concordance across the 27-patient cohort. While requiring independent validation, this simplified approach highlights the translational potential of our findings and could evolve into a practical tool to guide MCL management and optimize therapeutic selection.

Discussion

MCL is an uncommon subtype of B-cell lymphoma, accounting for 4–9% of non-Hodgkin lymphoma in high-income countries (14). Multiple groundbreaking studies have already profiled the genomic, transcriptomic, and epigenetic landscapes of MCL (1-6, 15, 16), shedding light on its molecular heterogeneity, pathogenesis, and mechanisms of drug resistance. However, no comprehensive proteomic profiling of MCL had been reported to date. Hence, we addressed that gap by integrating proteomics with genomics and transcriptomics in primary MCL samples. Our analysis yielded the first proteogenomic atlas of MCL, uncovering potential biology and defining molecular subgroups with relatively distinct features and outcomes.

Our proteomic profiling of MCL cells revealed widespread pathway dysregulation. Proteins involved in metabolism, spliceosome, and DNA replication/repair were upregulated, underscoring enhanced genetic information processing. These alterations implicate that aberrant post-transcriptional regulation and genomic instability as central to MCL pathogenesis and its high proliferative activity. Conversely, pathways related to cellular structure and immune function were broadly downregulated,

including MAPK signaling, cytoskeletal organization, cell adhesion, and immune effector responses. *FERMT3* downregulation might impair stromal adhesion and immune recognition, thereby promoting tumor cell migration and resistance to cytotoxic killing. Similarly, reduced S100A8/9 in tumor cells might reflect an immunosuppressive niche, as these proteins are known to modulate inflammation. These findings point to impaired immune surveillance, weakened cytotoxic function, and diminished intercellular junctions together facilitate immune evasion and systemic dissemination in MCL.

The spliceosome, a crucial component in the generation of mature mRNA and an important post-transcriptional regulatory mechanism (17-19), was significantly upregulated at both RNA and protein levels in MCL. Clinical and mechanistic studies have confirmed that mutations affecting the spliceosome or splicing factors are recurrent genetic abnormalities in various cancers. For example, the *SF3B1* mutation is commonly observed in myeloid malignancies and CLL (20-22). Such spliceosome alterations disrupt key cellular signaling pathways, including those involved in DNA damage response and B-cell signaling, driving tumorigenesis and drug resistance (17, 23, 24). A large-scale genomic study reported novel mutations in RNA-binding proteins in MCL, including *HNRNPH1*, which regulates alternative pre-mRNA splicing and is associated with poor prognosis (6). Elevated expression levels of HNRNPH proteins were also observed. In our study, we found significant upregulation of genes or proteins associated with spliceosome components, such as *DDX39B*, *SNRPB*, *U2AF1*, *SF3B4*, and *SF3A2*, supporting spliceosome dysregulation as a common pathogenic feature in MCL. Additionally, our differential protein expression analysis showed that the spliceosome pathway was downregulated in patients with IGHV-mutated status and *CCND1* mutations. In previous research, we identified that MCL patients harboring these two mutations represent a distinctive subset with favorable outcomes. Thus, the upregulation of spliceosome pathway may represent the high-risk biology of MCL. Investigating whether targeting spliceosome abnormalities could provide therapeutic benefits in specific MCL subgroups warrants further exploration. Although we identified spliceosome dysregulation as a hallmark of MCL, the present study did not comprehensively characterize specific alternative splicing isoforms or structural variants. Further investigations into these splicing aberrations and their mechanistic contributions to MCL pathogenesis are currently underway.

Functional protein abundance cannot be reliably inferred from transcriptional data alone, due to extensive post-transcriptional regulation (25-28). In our cohort, the correlation between RNA and protein in MCL was also limited (the median correlation coefficient of 0.377). This value is similar to previous studies that reported comparable RNA-protein correlation levels in other cancers, such as 0.18 in CLL, 0.31 in acute myeloid leukemia, 0.39 in breast cancer, and 0.47 in colorectal cancer

(9-11, 26). Gene expression is shaped by multi-layered controls encompassing mRNA transcription, processing, transport, translation, modification, and degradation (25, 28). Dysregulation at any stage of these processes may mediate or affect the occurrence of various diseases, like cancer (29-31). These findings reveal a dual regulatory mechanism in tumors: while tight transcription-translation coupling supports the proliferative and metabolic demands of tumor cells, extensive post-transcriptional regulation simultaneously drives dysregulated cell cycle progression and impairs DNA repair. Consequently, relying solely on mRNA measurements may misrepresent the functional state of these pathways.

Notably, aggressive MCL subtypes exhibited higher mRNA-protein correlation (Figure S5 and S11). We hypothesize that highly proliferative tumors maintain tight transcriptional-translational coupling to meet the metabolic and structural demands of rapid growth, minimizing post-transcriptional buffering as an adaptive strategy. This heightened coupling may render aggressive cells particularly vulnerable to proteotoxic stress, providing a mechanistic rationale for the efficacy of proteasome inhibitors in this context. Conversely, the lower concordance in indolent cases likely reflects a more quiescent state with greater post-transcriptional buffering or protein turnover. These insights underscore the power of multi-omics integration can delineate aggressive MCL phenotypes beyond genomics alone.

In our prior publication, we have described different subgroups of MCL based on genomic data (5). The integration of multiple omics layers (DNA, RNA, and protein data) into a unified classification model resulted in a higher C-index, indicating better prognostic accuracy for MCL patients. This is quite promising for a 27-patient discovery dataset. If validated, this refined stratification will provide a more nuanced molecular landscape with therapeutic implications. For C1 group, there was no change between single-omics and multi-omics. This group, featured by mutated IGHV and *CCND1* and hyperactive BCR signaling and OXPHOS pathways, suggesting potential sensitivity to BTK or OXPHOS inhibitors. C2 was enriched with *NSD2* mutations. Jain et al. reported that *NSD2* mutations may be associated with blast transformation and resistance to ibrutinib alone (32). In contrast, the C3 and C4 group, characterized by *TP53* abnormalities and *del9p*, had the worst clinical outcome. This result is consistent with previous studies (33-35). C3 and C4 were mainly downregulated in immune-related pathways, implying that these clusters may be associated with immune-evasive phenotypes. But C4 had a greater emphasis on unchecked cell cycle progression and replicative stress, whereas C3 showed a shift toward metabolic adaptation and adhesion. High proliferative activity and immune escape may jointly contribute to the extremely poor prognosis of C4. It also raises the possibility that immune-based therapies, like bispecific antibodies or CAR T-therapy, might be less effective unless combined with strategies to reverse that immune-cold state. On the other

hand, the strong cell cycle and DNA repair signals in cluster C4 suggest vulnerability to cell cycle kinase inhibitors (e.g., CDK4/6 inhibitors) or DNA damage exacerbation (e.g., ATR inhibitors). Collectively, this multi-omics landscape refines risk stratification and provides a basis for future precision medicine approaches in MCL.

We acknowledge several limitations in our study. First, our clustering was derived from a relatively small cohort of 27 MCL patients and lacks independent validation due to the rarity of the disease and the difficulty in obtaining high-purity samples. Furthermore, our cohort was exclusively constituted of male patients with peripheral blood involvement. While this design allowed for a focused analysis of tumor cell-intrinsic proteomic differences, it implies that caution should be exercised when extrapolating our findings to pure nodal disease or female patients. Finally, despite the high sensitivity of DIA-MS, the technique is subject to methodological constraints. Due to differences in protein abundance and potential masking effects, it is not possible to detect every expressed protein within the cellular proteome.

Nonetheless, our study presents a comprehensive proteogenomic characterization of MCL. By integrating multi-omics data, we identified four molecular subtypes and demonstrated that proteomic information substantially improves risk stratification. Biologically, we highlighted the prominence of the spliceosome and other post-transcriptional modulators in MCL, suggesting new avenues for therapeutic intervention. This work establishes the unique biological and clinical value of protein abundance data in MCL. Additionally, we provide a comprehensive protein expression reference map to support future research and translational efforts.

Conflict of Interest

The authors declare no competing financial interests.

Author Contributions

SHY and LLW conceptualized the study design. YTY collected samples, performed experiments and created graphs, WHC and YTY wrote the manuscript. YYT, XZG, JS, JL, MK, and PP conducted data analysis and statistics. XYZ, YY, TYW, WJX, DHZ, GA, MH, and ZY acquired the data and managed the patients. LLW, LGQ, JWQ and SHY revised the manuscript critically and approved the final version.

Acknowledgements

This work was supported by grants from the National Nature Science Foundation of China (82570248,82170193,82370197,82200215), the Chinese Academy of Medical Sciences Innovation Fund for Medical Sciences (2025-I2M-C&T-B-073), Beijing Xisike Clinical Oncology Research Foundation (Y-2024AZ(BTK)ZD--0074) and the Shenzhen Science and Technology Innovation Commission (JCYJ20240813140803005).

Figure Legends

Figure 1: Differential Analysis of MCL and Normal B Cells at the Proteomic and Transcriptomic Levels. (A) Workflow of integrative analysis based on proteogenomics and clinical outcomes. **(B)** Volcano plot displaying differentially expressed proteins in MCL compared to normal B cells (n=5702). **(C)** Functional enrichment analysis of differentially expressed proteins in MCL compared to normal B cells. **(D)** UpSet plot illustrating the overlap of differentially expressed genes between transcriptomics and proteomics. **(E)** Pathway enrichment analysis of co-upregulated and co-downregulated genes at both transcript and protein levels. **(F)** Perform GSEA analysis on differentially expressed genes from proteomics and transcriptomics, calculate the enrichment *P*-values for each pathway, and plot a scatter plot showing the Pearson correlation of enrichment *P*-values for the two omics. The red pathways represent the signaling pathways that are significantly upregulated at both multi-omics

levels in MCL cells, while the blue pathways represent the signaling pathways that are significantly downregulated at both multi-omics levels in MCL cells.

Figure 2: The impact of genetic aberrations on differential protein expression and its enrichment pathways in MCL. **(A)** Workflow diagram. **(B)** Number of differentially expressed proteins associated with key genetic aberrations (*P*<0.05). **(C)** Volcano plot illustrating significantly upregulated and downregulated proteins in IGHV-mutated versus IGHV-unmutated MCL patients. **(D)** Enriched pathways of differential protein expression in IGHV-mutated patients. **(E)** Enriched pathways of differential protein expression in *CCND1*-mutated patients.

Figure 3: Protein-mRNA concordance and its impact on outcomes in MCL. (A) Pearson correlation distribution between protein and RNA expression across 5222 genes. **(B)** Ranked correlation coefficients for each protein. **(C)** Enrichment analysis of high-correlation genes (r>0.6). **(D)** Enrichment analysis of low-correlation genes (r<0.3).

Figure 4: Gene set associated with MCL survival prognosis. (A) Volcano plot of prognostic mRNAs from univariate Cox analysis ($P < 0.05$), showing 1821 mRNAs associated with longer survival (HR < 1, blue) and 1678 mRNAs associated with shorter survival (HR > 1, red). **(B)** Volcano plot of prognostic proteins from univariate Cox analysis ($P < 0.05$), showing 347 proteins associated with longer survival (HR < 1, blue) and 602 proteins associated with shorter survival (HR > 1, red). **(C)** Venn diagram showing overlap between transcriptomic and proteomic data in the identification of mutual prognostic genes. A total of 252 prognostic genes were identified, with 141 associated with poor prognosis both in RNA and protein level (Gene set A, $P < 0.05$, HR > 1) and 92 associated with favorable prognosis both in RNA and protein level (Gene set B, $P < 0.05$, HR < 1). **(D)** Enrichment analysis of Gene set A (poor prognostic factors). **(E)** Enrichment analysis of Gene set B (favorable prognostic factors).

Figure 5: The identification of four molecular subgroups based on integrated multi-omics clustering and clinical implications in MCL. (A) Unsupervised clustering of multi-omics profiles reveals patient clusters. The heatmap visualizes the top discriminant RNA and protein signatures associated with each subgroup. Color scale represents Z-score normalized expression values. **(B)** Sankey diagram showing redistribution of clusters between the clustering based on single-omics and the clustering based on multi-omics. The width of each band is proportional to the number of patients. **(C)** Progression-free survival (PFS) and overall survival (OS) between four subgroups based on single-omics clustering (PFS: $P = 0.006$; OS: $P = 0.008$) and multi-omics clustering (PFS: $P < 0.001$; OS: $P < 0.001$). **(D)** Simplified multi-omics clustering incorporating representative 7 genetics, 7 RNA

and 3 protein signatures.

Reference

1. Kridel R, Meissner B, Rogic S, Boyle M, Telenius A, Woolcock B, et al. Whole transcriptome sequencing reveals recurrent NOTCH1 mutations in mantle cell lymphoma. Blood. 2012;119(9):1963-71.

2. Beà S, Valdés-Mas R, Navarro A, Salaverria I, Martín-Garcia D, Jares P, et al. Landscape of somatic mutations and clonal evolution in mantle cell lymphoma. Proceedings of the National Academy of Sciences of the United States of America. 2013;110(45):18250-5.

3. Zhang J, Jima D, Moffitt AB, Liu Q, Czader M, Hsi ED, et al. The genomic landscape of mantle cell lymphoma is related to the epigenetically determined chromatin state of normal B cells. Blood. 2014;123(19):2988-96.

4. Nadeu F, Martin-Garcia D, Clot G, Díaz-Navarro A, Duran-Ferrer M, Navarro A, et al. Genomic and epigenomic insights into the origin, pathogenesis, and clinical behavior of mantle cell lymphoma subtypes. Blood. 2020;136(12):1419-32.

5. Yi S, Yan Y, Jin M, Bhattacharya S, Wang Y, Wu Y, et al. Genomic and transcriptomic profiling reveals distinct molecular subsets associated with outcomes in mantle cell lymphoma. The Journal of clinical investigation. 2022;132(3).

6. Pararajalingam P, Coyle KM, Arthur SE, Thomas N, Alcaide M, Meissner B, et al. Coding and noncoding drivers of mantle cell lymphoma identified through exome and genome sequencing. Blood. 2020;136(5):572-84.

7. Johansson HJ, Socciarelli F, Vacanti NM, Haugen MH, Zhu Y, Siavelis I, et al. Breast cancer quantitative proteome and proteogenomic landscape. Nature communications. 2019;10(1):1600.

8. Zhang H, Liu T, Zhang Z, Payne SH, Zhang B, McDermott JE, et al. Integrated Proteogenomic Characterization of Human High-Grade Serous Ovarian Cancer. Cell. 2016;166(3):755-65.

9. Mertins P, Mani DR, Ruggles KV, Gillette MA, Clauser KR, Wang P, et al. Proteogenomics connects somatic mutations to signalling in breast cancer. Nature. 2016;534(7605):55-62.

10. Meier-Abt F, Lu J, Cannizzaro E, Pohly MF, Kummer S, Pfammatter S, et al. The protein landscape of chronic lymphocytic leukemia. Blood. 2021;138(24):2514-25.

11. Kramer MH, Zhang Q, Sprung R, Day RB, Erdmann-Gilmore P, Li Y, et al. Proteomic and phosphoproteomic landscapes of acute myeloid leukemia. Blood. 2022;140(13):1533-48.

12. Akbani R, Ng PK, Werner HM, Shahmoradgoli M, Zhang F, Ju Z, et al. A pan-cancer proteomic perspective on The Cancer Genome Atlas. Nature communications. 2014;5:3887.

13. Wang B, Mezlini AM, Demir F, Fiume M, Tu Z, Brudno M, et al. Similarity network fusion for aggregating data types on a genomic scale. Nat Methods. 2014;11(3):333-7.

14. Vose JM. Mantle cell lymphoma: 2017 update on diagnosis, risk-stratification, and clinical management. American journal of hematology. 2017;92(8):806-13.

15. Agarwal R, Chan YC, Tam CS, Hunter T, Vassiliadis D, Teh CE, et al. Dynamic molecular monitoring reveals that SWI-SNF mutations mediate resistance to ibrutinib plus venetoclax in

mantle cell lymphoma. Nature medicine. 2019;25(1):119-29.

16. Zhang L, Yao Y, Zhang S, Liu Y, Guo H, Ahmed M, et al. Metabolic reprogramming toward oxidative phosphorylation identifies a therapeutic target for mantle cell lymphoma. Science translational medicine. 2019;11(491).

17. Wang E, Aifantis I. RNA Splicing and Cancer. Trends in cancer. 2020;6(8):631-44.

18. Obeng EA, Stewart C, Abdel-Wahab O. Altered RNA Processing in Cancer Pathogenesis and Therapy. Cancer discovery. 2019;9(11):1493-510.

19. Yang H, Beutler B, Zhang D. Emerging roles of spliceosome in cancer and immunity. Protein & cell. 2022;13(8):559-79.

20. Palomo L, Meggendorfer M, Hutter S, Twardziok S, Ademà V, Fuhrmann I, et al. Molecular landscape and clonal architecture of adult myelodysplastic/myeloproliferative neoplasms. Blood. 2020;136(16):1851-62.

21. Quesada V, Conde L, Villamor N, Ordóñez GR, Jares P, Bassaganyas L, et al. Exome sequencing identifies recurrent mutations of the splicing factor SF3B1 gene in chronic lymphocytic leukemia. Nature genetics. 2011;44(1):47-52.

22. Li Z, He Z, Wang J, Kong G. RNA splicing factors in normal hematopoiesis and hematologic malignancies: novel therapeutic targets and strategies. Journal of leukocyte biology. 2023;113(2):149-63.

23. Wang L, Brooks AN, Fan J, Wan Y, Gambe R, Li S, et al. Transcriptomic Characterization of

SF3B1 Mutation Reveals Its Pleiotropic Effects in Chronic Lymphocytic Leukemia. Cancer cell. 2016;30(5):750-63.

24. Ten Hacken E, Valentin R, Regis FFD, Sun J, Yin S, Werner L, et al. Splicing modulation sensitizes chronic lymphocytic leukemia cells to venetoclax by remodeling mitochondrial apoptotic dependencies. JCI insight. 2018;3(19).

25. Vogel C, Marcotte EM. Insights into the regulation of protein abundance from proteomic and transcriptomic analyses. Nature reviews Genetics. 2012;13(4):227-32.

26. Zhang B, Wang J, Wang X, Zhu J, Liu Q, Shi Z, et al. Proteogenomic characterization of human colon and rectal cancer. Nature. 2014;513(7518):382-7.

27. Liu Y, Beyer A, Aebersold R. On the Dependency of Cellular Protein Levels on mRNA Abundance. Cell. 2016;165(3):535-50.

28. Buccitelli C, Selbach M. mRNAs, proteins and the emerging principles of gene expression control. Nature reviews Genetics. 2020;21(10):630-44.

29. Lin S, Gregory RI. MicroRNA biogenesis pathways in cancer. Nature reviews Cancer. 2015;15(6):321-33.

30. Tahmasebi S, Khoutorsky A, Mathews MB, Sonenberg N. Translation deregulation in human disease. Nature reviews Molecular cell biology. 2018;19(12):791-807.

31. Delaunay S, Helm M, Frye M. RNA modifications in physiology and disease: towards clinical applications. Nature reviews Genetics. 2024;25(2):104-22.

32. Jain P, Kanagal-Shamanna R, Zhang S, Ahmed M, Ghorab A, Zhang L, et al. Long-term outcomes and mutation profiling of patients with mantle cell lymphoma (MCL) who discontinued ibrutinib. British journal of haematology. 2018;183(4):578-87.

33. Clot G, Jares P, Giné E, Navarro A, Royo C, Pinyol M, et al. A gene signature that distinguishes conventional and leukemic nonnodal mantle cell lymphoma helps predict outcome. Blood. 2018;132(4):413-22.

34. Ferrero S, Rossi D, Rinaldi A, Bruscaggin A, Spina V, Eskelund CW, et al. KMT2D mutations and TP53 disruptions are poor prognostic biomarkers in mantle cell lymphoma receiving high-dose therapy: a FIL study. Haematologica. 2020;105(6):1604-12.

35. Delfau-Larue MH, Klapper W, Berger F, Jardin F, Briere J, Salles G, et al. High-dose cytarabine does not overcome the adverse prognostic value of CDKN2A and TP53 deletions in mantle cell lymphoma. Blood. 2015;126(5):604-11.

589 **Table 1. Baseline characteristics of patients**

Characteristics	MCL patients (n=27)
Age, years (median, range)	57 (44–79)
Male, n (%)	27 (100)
Lactate dehydrogenase >ULN	18 (66.7)
ECOG-PS score >1	6 (22.2)
WBC at diagnosis, × 10^9 /L, median (range)	82.0 (11.8–836.0)
Hemoglobin at diagnosis, g/dl, median (range)	11.5 (5.0–14.9)
Platelet at diagnosis, × 10^9/L, median (range)	101 (40–362)
Malignant cells fraction in BM detected by FCM, median (range)	73.2 (38.5–95.1)
Clinical group, n (%)	
nnMCL	6 (22)
cMCL	21 (78)
Pathology, n (%)	
Blastic	2 (8)
Classic	23 (92)
No tested	2
IGHV status, n (%)	
Mutated	7 (26)
Unmutated	20 (74)
MIPI score, n (%)	
Low risk	0 (0)
Intermediate risk	7 (26)
High risk	20 (74)

590 Abbreviations: ULN, upper limit of normal; ECOG-PS, Eastern Cooperative Oncology Group Performance Status;
591 WBC, white blood cell; BM, bone marrow; FCM, flow cytometry; nnMCL, indolent leukemic non-nodal mantle cell
592 lymphoma; cMCL, conventional mantle cell lymphoma; IGHV, immunoglobulin heavy chain variable; MIPI, Mantle Cell
593 Lymphoma International Prognostic Index.
594

Figure 1

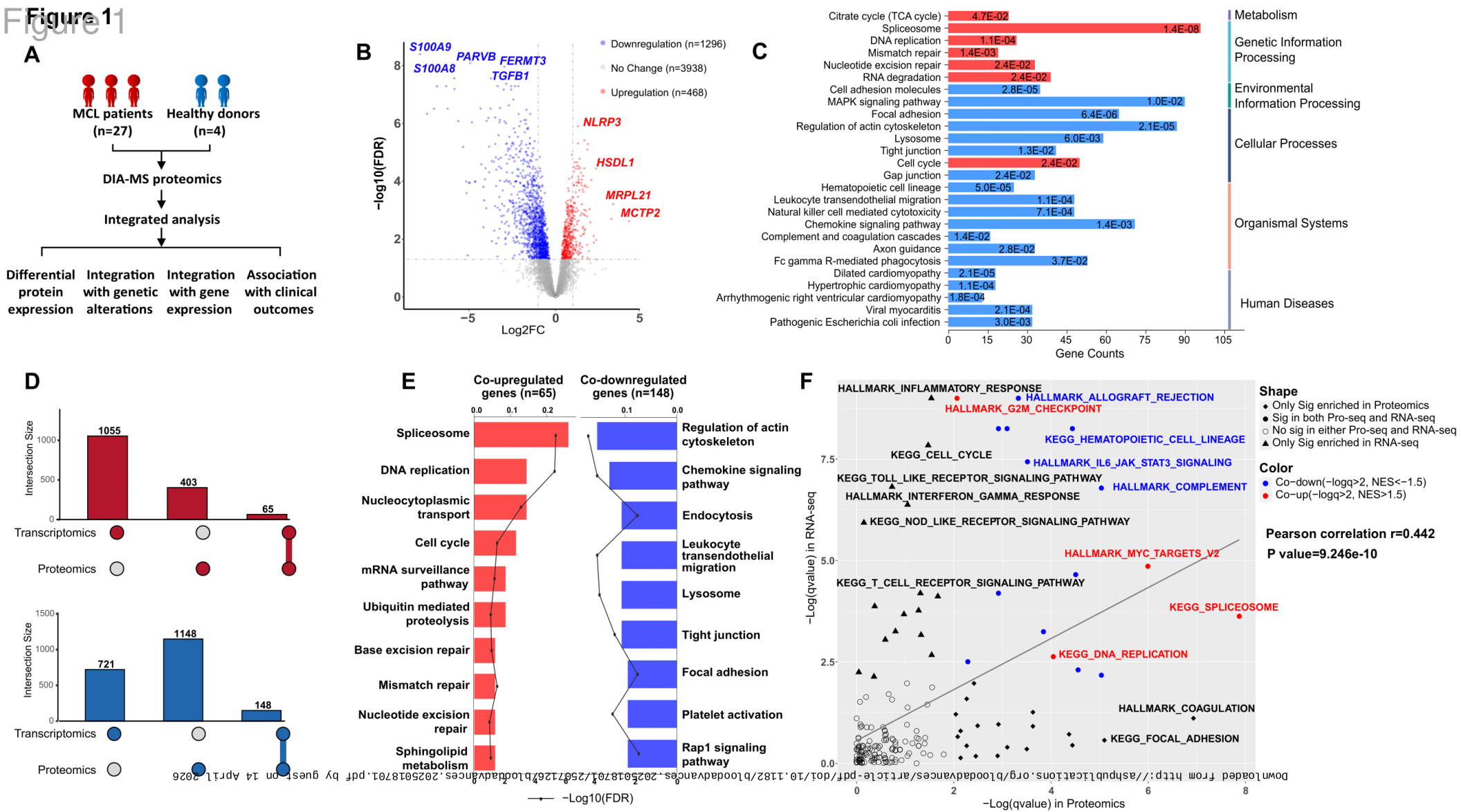

Figure 2

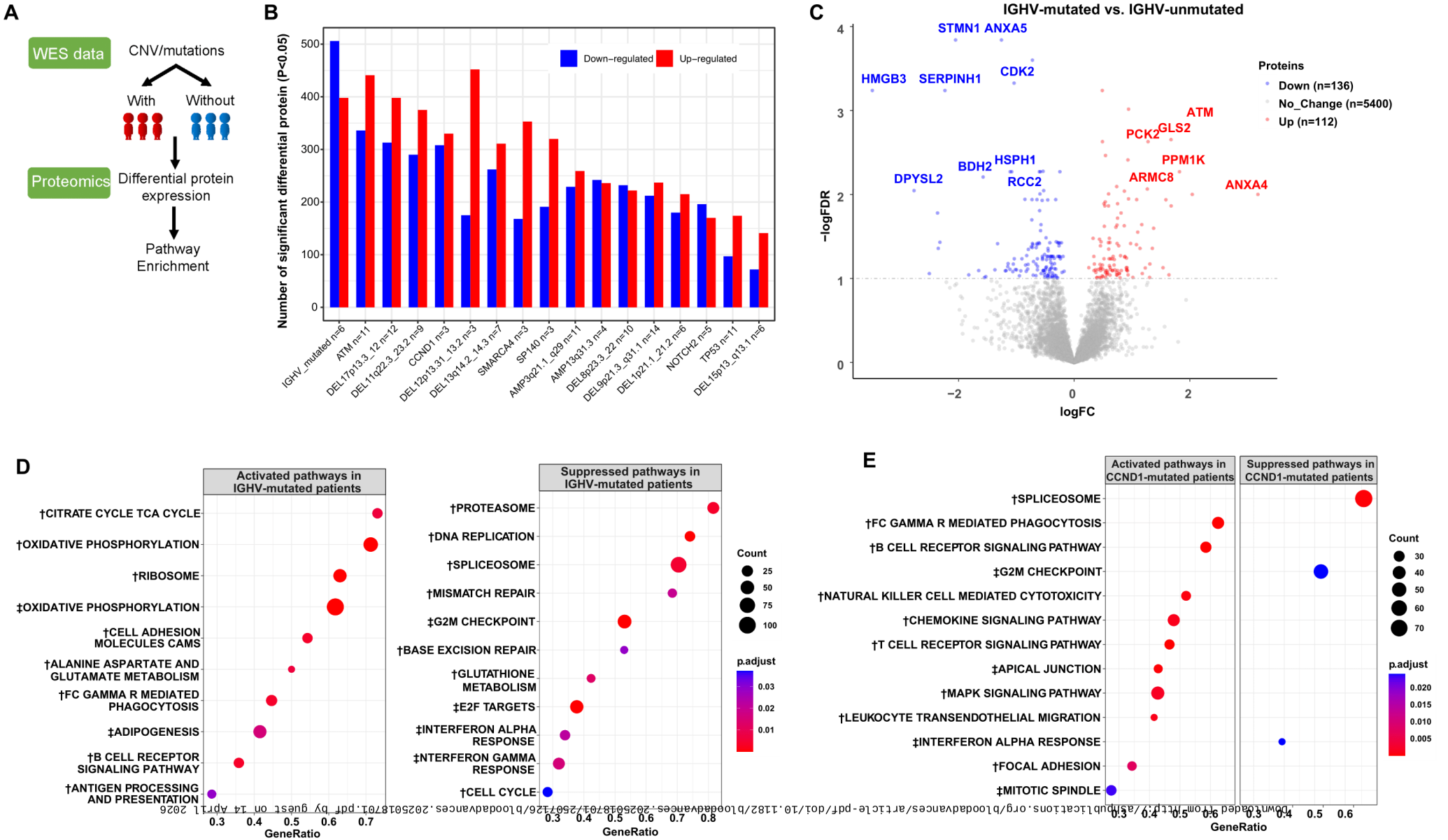

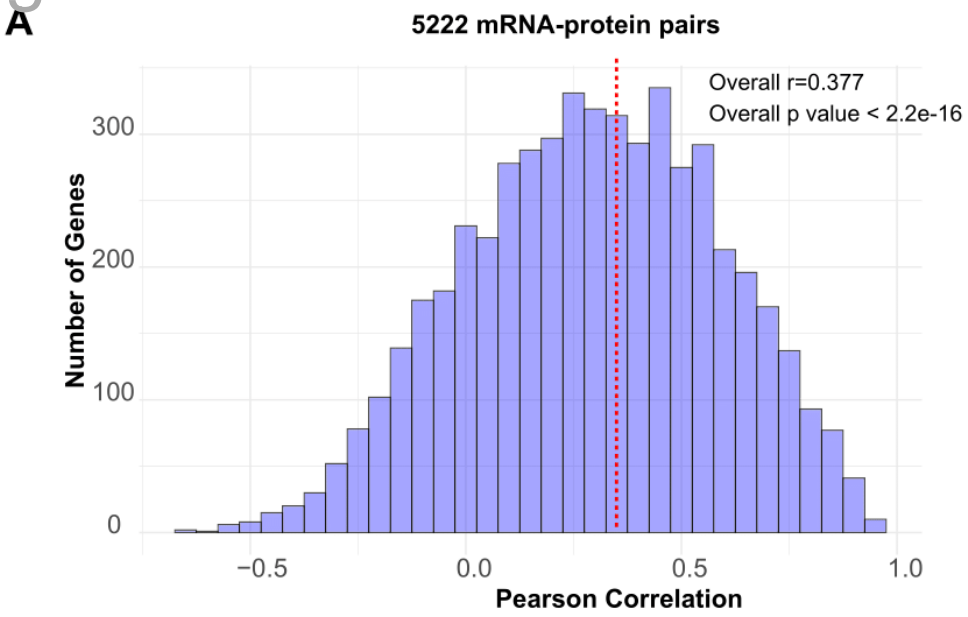

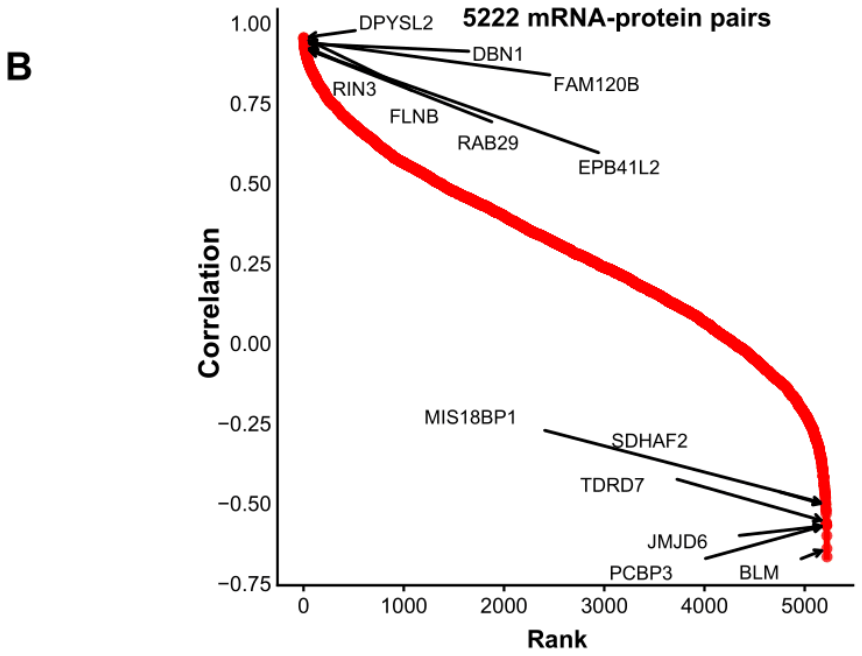

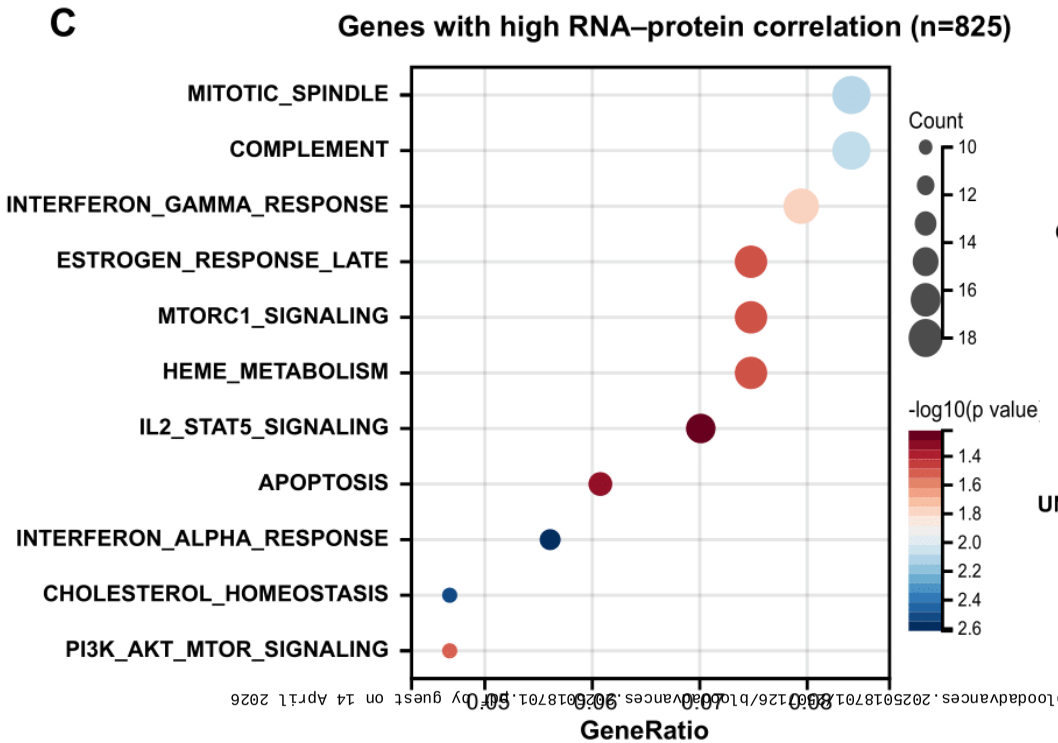

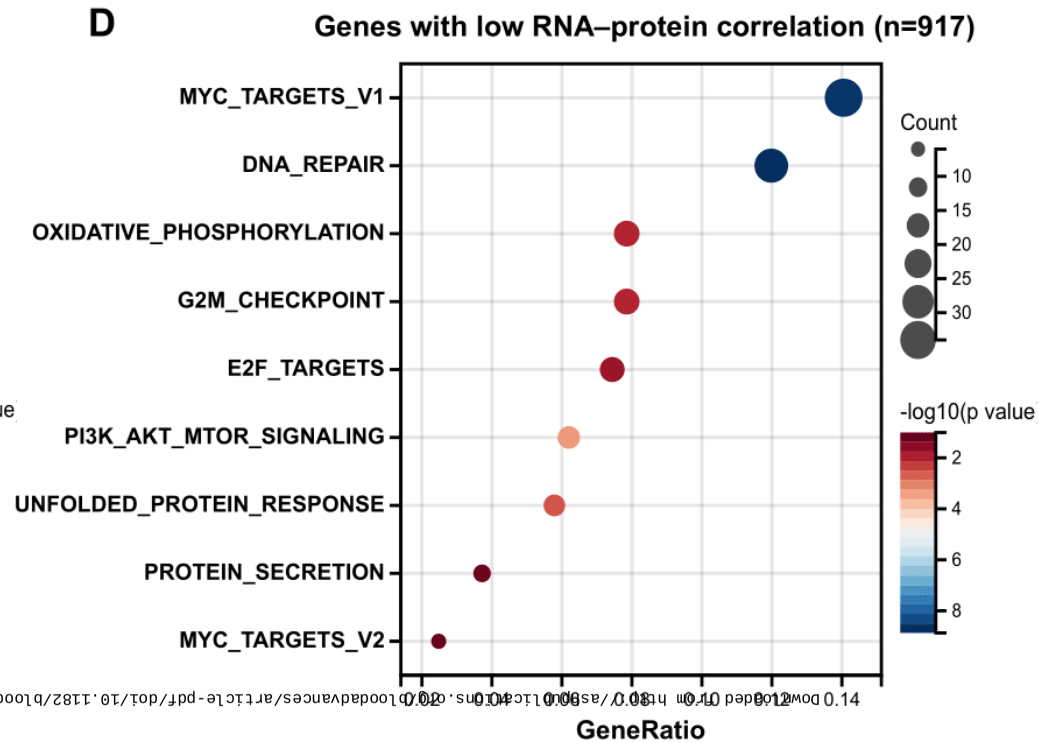

Figure 4